Supplement to "Scaled seismotectonic models of megathrust seismic cycles through the lens of dynamical system theory"

Corbi F.[1], Gualandi A.[2], Mastella G.[3], Funiciello F.[4]
[1]Istituto di Geologia Ambientale e Geoingegneria - CNR c/o Dipartimento di Scienze della Terra, Sapienza Università di Roma, Rome, Italy.
[2] Bullard Laboratories, Department of Earth Science, University of Cambridge, UK.
[3] Sapienza University of Rome, Earth Sciences, Rome, Italy.
[4] Dipartimento di Scienze, Laboratory of Experimental Tectonics, Università "Roma TRE", Rome, Italy.

Contents of this file
This supplementary information file consists of 6 sections detailing the methodologies utilized, 16 figures supporting the main research, and 1 table outlining experimental details.

Text S0: Methods

Embedding Theory ET attempts to reconstruct the phase-space of the system from the trajectory of a single observable. The phase-space has a number of axes equal to the number of variables that describe the system's behavior. It allows us to depict every possible state of the system. The trajectory followed by the system in the phase space fully defines it. If the observation time is long enough, so that the ergodic assumption can be made, and the sampling rate is high enough to illuminate the process, it is possible to reconstruct a shadow of the original trajectory even if we have access to the evolution of the system on only a subset of the actual phase space [Takens, 1981]. This theoretical result is particularly powerful in real-case circumstances, where access to all possible variables is often problematic. We use the method of time delays [Takens, 1981]. The procedure involves duplicating the original time-series m times with a τ time-step shift between each copy. The hyper-parameters m and τ are named embedding dimension and time delay, respectively. The reconstructed time delay vectors can be written as

$$F(t,\tau,m) = [x(t),x(t-\tau),\ldots,x(t-(m-1)\,\tau)] \quad \text{(eq.1)}$$

where x is the analyzed signal and $t = 1, 2, \cdots, N - (m - 1)\tau$, with N being the total length of the time series (Figure 2B). $F(t,\tau,m)$ represents an m-dimensional vector delaying in time the time series x(t) of an amount τ for $m - 1$ times.

The appropriate selection of observables (e.g., displacement) and hyper-parameters produces a reconstructed trajectory in the delay coordinate space to be topologically similar (i.e., preserve shape characteristic) to the signal in the original phase space (Figure 2C). We determine the value of τ by using the Average Mutual Information (AMI; SI text2) and the value of m using the method of Cao [1997; SI text3]. Once m is known we can refer to Taken's theorem [1981] and estimate the system dimension D. Taken's theorem states that the embedding dimension m must be at least larger than twice the true dimension D (i.e., $m \geq 2D+1$) of the underlying system. If the functions governing the dynamics are sufficiently smooth, certain properties can be preserved with values of m smaller than 2D, except for subsets of dimension size no greater than 2D - m - 1 [Sauer et al., 1991]. Cao's method [1997] allows us to determine the minimum embedding dimension, which cannot be smaller than D (i.e., $D \leq m$). Thus, once m is determined, we can set bounds on the true dimension of the system as $(m-1)/2 \leq D \leq m$.

The dimension estimated via ET provides an overall, time-averaged, value for the whole system dynamics. Since the stick-slip behavior of seismotectonic models is by nature characterized by instabilities, the dimension of the trajectory may be time-dependent. To analyze the dynamics of the experiments over time we use a method that applies Extreme Value Theory EVT to dynamical system theory [Faranda et al., 2017; SI text5]. We use two properties: the instantaneous dimension (d1) and the instantaneous extremal index (θ). To estimate these quantities, we use the complete spatio-temporal information (i.e. no embedding is used) and we assume that the state ζ of the system is described by a specific configuration of the chosen variable (e.g., displacement field). The instantaneous dimension $d1(\zeta)$ measures the density of neighboring points (i.e., similar configurations) in the phase space. The system dimension D is obtained by averaging *d1* over all ζ. The "stickiness" of the state ζ allows us to estimate $\theta(\zeta)$, which is defined as the inverse of the average persistence time of trajectories around ζ and is normalized between 0 and 1. Lower values of θ reflect a persistent state and higher values a transient one.

$\theta(\zeta)$ is related to the metric entropy H of the system, and thus to its predictability. In fact, H is equal to the sum of all positive Lyapunov exponents, and we can thus use its inverse to get an equivalent of the Lyapunov time but using all directions of divergence. As in Gualandi et al. [2020], we use two approaches to estimate H and the corresponding predictability horizon t*. The first method uses the following relation between the extremal index $\boldsymbol{\Theta}$ and the entropy H: $\boldsymbol{\Theta} \sim 1 - e^{-H}$; with $\boldsymbol{\Theta} \in [\theta min, \theta max]$ [Faranda and Vaienti, 2018]. The second method is based on Nonlinear Forecasting Analysis (NFA) [Farmer and Sidorowich, 1987; Wales, 1991]. To make a prediction of Tp time steps in the future, we split our time series into two parts of equal duration. The first half of the time series (training set) is used to learn a nonlinear map using a local linear approximation in the phase space. The second half of the time series (test set) is used to test the "performances" of predictions, quantified as ρ i.e., the correlation between the observed and predicted time series at different Tp [Wales, 1991]; and $\boldsymbol{\epsilon}$ i.e., the root mean square error between observed and predicted time series normalized by the root mean square deviation from zero [Farmer and Sidorowich, 1987]. Since ρ and $\boldsymbol{\epsilon}$ provide different values of H, t*NFA=1/H will either refer to ρ (i.e., t*ρ) or to $\boldsymbol{\epsilon}$ (i.e., t*$\boldsymbol{\epsilon}$; SI text4). t*EVT and t*NFA are complementary in a way that the former represents a "global" measure and the latter, being computed for a precise point along the sampled section, refers to a particular location on the model surface.

Text S1: Data and data pre-processing

Table S1 reports information about monitoring of our experiments and image processing. The PIV provides us with velocity field time series. These are integrated to obtain displacement time series. One can use either the velocity or the displacement to build the delay embedding. Here we select the trench orthogonal component of the displacement as the target signal, that we indicate with x(t). PIV also provides the trench parallel component of the velocity field, which we ignore in this study as the kinematically imposed loading (i.e., plates convergence) in our experiments is perpendicular to the trench. The temporal pattern of x(t) clearly depicts stick-slip dynamics. Preliminary analysis supported our choice of using displacement rather than velocity for the reconstruction of model dynamics.

First, all displacement time series have been normalized to zero mean and unit variance to ensure the same level of magnitude for comparison. Second, linear and second order polynomial trends have been removed by simple regression to make the stick-slip confined in a given range and avoid non-stationary behavior. Time series data are not passed through filters (e.g., smoothing or moving average), to prevent potential influence on the reconstructed dynamics [Badii et al., 1988; Theiler and Eubank, 1993]. Figures S1-S4 show displacement time series for all experiments.

Text S2: Average mutual information AMI

The Average Mutual Information (AMI) is a widely used technique to determine the ideal time delay (τ) needed for phase space reconstruction. AMI quantifies the relation between x(t + τ) and x(t), at a particular τ. To calculate the AMI of a time series x (t), first an histogram with a given number of bins is created. In this study we used 10 bins. We define P_i the probability that the signal has a value inside the i^{th} bin, and $P_{ij}(\tau)$ the probability that x(t) is in bin i and x(t+τ) is in bin j. Next, AMI for τ time delay is computed as $AMI(\tau)= \sum_{i,j}P_{i,j}\log(P_{ij}/P_iP_j)$. We select the first local minimum of AMI (τAMI) as the optimum delay. To investigate how our assessment of the embedding dimension is affected by our ability to identify this minimum, we implement 5 different values of τ from a linearly spaced selection in the [0.5*τAMI, 1.5*τAMI] range. To compute AMI we used the Matlab function *phaseSpaceReconstruction*. We report all AMI(τ) for all experiments in Figure S13-S16. Plots of AMI(τ) (realized using the *ARFM_ami.m* function [Sujith, 2019]) have been used for visual inspection.

Text S3: Cao's method for calculating the minimum embedding dimension

We used the method of Cao to calculate the optimum embedding dimension [Cao, 1997]. The algorithm uses the embedding function F and detects false neighbors in the reconstructed phase space when changing embedding dimension m. False neighbors are points in a lower dimensional embedding of a dynamical system that appear close together, but are actually far apart in the higher dimensional phase space. The quantities E and E* are defined as follows:

$$E(m) = \frac{1}{T - m\tau} \sum_{t=1}^{T-m\tau} \frac{\| F(t,\tau,m+1) - F_{n(t,m)}(t,\tau,m+1) \|}{\| F(t,\tau,m) - F_{n(t,m)}(t,\tau,m) \|}$$

(eq.2)

$$E^{*}(m) = \frac{1}{T - m\tau} \sum_{t=1}^{T-m\tau} \| x(t+m\tau) - x_{n(t,m)}(t+m\tau) \|$$

(eq.3)

where $1 \leq n(t,m) \leq (T-m)$ and $F_{n(t,m)}(t,\tau,m)$ is the nearest neighbor of $F(t,\tau,m)$. From E and E^* two following ratios can be defined:

$$E_1(m) = \frac{E(m+1)}{E(m)}$$

(eq.4)

$$E_2(m) = \frac{E^{*}(m+1)}{E^{*}(m)}$$

(eq.5)

$E_1(m)$ reaches a plateau and stops changing once all the false neighbors are identified after a dimension m. We implement three thresholds (i.e., 0.900, 0.925 and 0.950) to identify the plateau and define then the minimum embedding dimension as m +1 (Figure S11). $E_2(m)$ is useful for determining whether the analyzed time series results from a deterministic or stochastic process. In the latter case, consecutive points in the timeserie are independent from previous ones and $E_2(m)$ =1 for each m (Figure S12). If the analyzed time series results from a deterministic process $E_2(m)$ is not constant and some $E_2(m) \neq 1$. To compute $E_1(m)$ and $E_2(m)$ we used the Matlab function *cao_deneme.m* by M. Kizilkaya. For each time series we computed 15 optimal embedding dimensions by systematically varying the 3 thresholds of E_1 and the 5 values of τ (SI text2).

Text S4: Estimating the prediction horizon form entropy

In the frame of dynamical systems theory, entropy H refers to a measure of regularity of fluctuations over time series data. Therefore, entropy is often associated with predictability. The prediction horizon t*, on the other hand, refers to the time window within which a model correctly predicts the future. It determines how far ahead the model predicts the future.

Here we used a basic nonlinear forecasting algorithm NFA based on the "Lorenz Method of Analogues". The idea behind the algorithm is that future states of the actual state's neighbors are indicative of the actual state's future [Lorenz, 1969]. NFA pseudo code can be found in Gualandi et al. [2020].

First, we split the analyzed time series in two parts of equal duration. We use the former (training set) to learn a nonlinear map to make a prediction Tp time steps in the future using a local linear approximation in the phase space. The second half of the time series (test set) is used to test the "performances" of predictions. We use the correlation between the observed and predicted time series at different Tp ρ and the root mean square error between observed and predicted time series normalized by the root mean square deviation from the mean of the observed time series $\boldsymbol{\epsilon}$ to quantify how well the NFA predicts the test set. Values of ρ and $\boldsymbol{\epsilon}$ at different Tp allow estimating H.

The first method to estimate H is based on the rate of loss of information from the time series and provides the following relationship: $\ln(1-\rho(Tp))=c+2HTp$. The number of points to use for the estimate is not strictly defined. Previous studies have used 2 or 6 points for example [Wales, 1991; Barraclough and De Santis, 1997]. Here, we used the first 3 points (i.e., Tp=1, 2, 3) of ρ to fit a linear model and estimate H. The resulting values of $t^*\rho=1/H$ for all analyzed time series are reported in Figure 5. A larger number of points (e.g. 4 points) provides a minor (i.e., ~ 1 frame) increase of $t^*\rho$ for the asperity area of both Gelquake and Foamquake.

The second method to estimate H is based on the following relation: $\ln \boldsymbol{\epsilon}(Tp)+2/D \ln N \approx \ln C+2HTp$; where D is the average attractor dimension from EVT and D is the number of datapoints, and holds for $\boldsymbol{\epsilon}<<1$. To compute H we used a linear fit for all values of $\boldsymbol{\epsilon}<0.3$ [e.g., Gualandi et al., 2020].

Since ρ and $\boldsymbol{\epsilon}$ provide different values of H, $t^*NFA=1/H$ will either refer to ρ (i.e., $t^*\rho$) or to $\boldsymbol{\epsilon}$ (i.e., $t^*\boldsymbol{\epsilon}$). Additionally, we provide an error t^*err for the estimation of t^* based on the standard error SE of the linear fit using the following relation $t^*err= t^{*2}(SE/2)$.

Text S5: Extreme Value Theory

We use the Extreme Value Theory EVT to compute two quantities of interest: the instantaneous dimension *d1* and the instantaneous extreme index θ.

d1 is informative of the number of variables needed to describe the dynamics of a system in a specific point of the phase space (i.e., a moment in time). The derivation of *d1* is based on the Poincarè theorem, specifically on the observation that if a point $\zeta(t)$ exists in the phase space, then after a sufficient amount of time the system will eventually revisit a region of the phase space arbitrarily close to $\zeta(t)$. *d1* defines the density of points $\zeta(t)$ in the phase space. For each $\zeta(t)$, the algorithm searches for the nearest configurations (i.e., nearby points in the phase space) and arranges them in order of their Euclidean distance from the current state. Successively it computes the negative log-distance from the current state. The distribution of negative log-distance can be represented by a generalized Pareto distribution GPD [Faranda et al., 2017]. The GPD shape parameter σ is the inverse of the instantaneous dimension $d(\zeta)=1/\sigma(\zeta)$. We can finally compute the attractor dimension D by calculating the temporal average of the instantaneous dimension d1.

The extremal instantaneous index θ is a measure of the inverse of the average persistence around a given state in a region of the phase space. In other words, θ informs us about the amount of time spent by a dynamical system in a given region of the phase space. θ ranges from 0 to 1, with smaller values representing a persistent state in the phase space and higher values representing states that will be rapidly abandoned. As a consequence θ can be related to predictability, in a way that large values of θ indicate less predictability. In fact, θ is related to entropy H [Faranda and Valenti, 2018]. We can introduce the extremal index $\boldsymbol{\Theta}$ (i.e., $\boldsymbol{\Theta} \in \theta min, \theta max$) and the following relation $\boldsymbol{\Theta} \sim 1 - e^{-H}$; we can thus derive the predictability horizon t*EVT as the inverse of the entropy. θ is calculated using the maximum likelihood estimator of Süveges (2007).

To summarize, *d1* is related to the density of points in a certain neighborhood of the phase space while θ indicates how long the system stays in a region of the phase space.

To compute *d1* and θ we used the Matlab function *fun_dynsys_univariate_analysis.m* by D. Faranda.

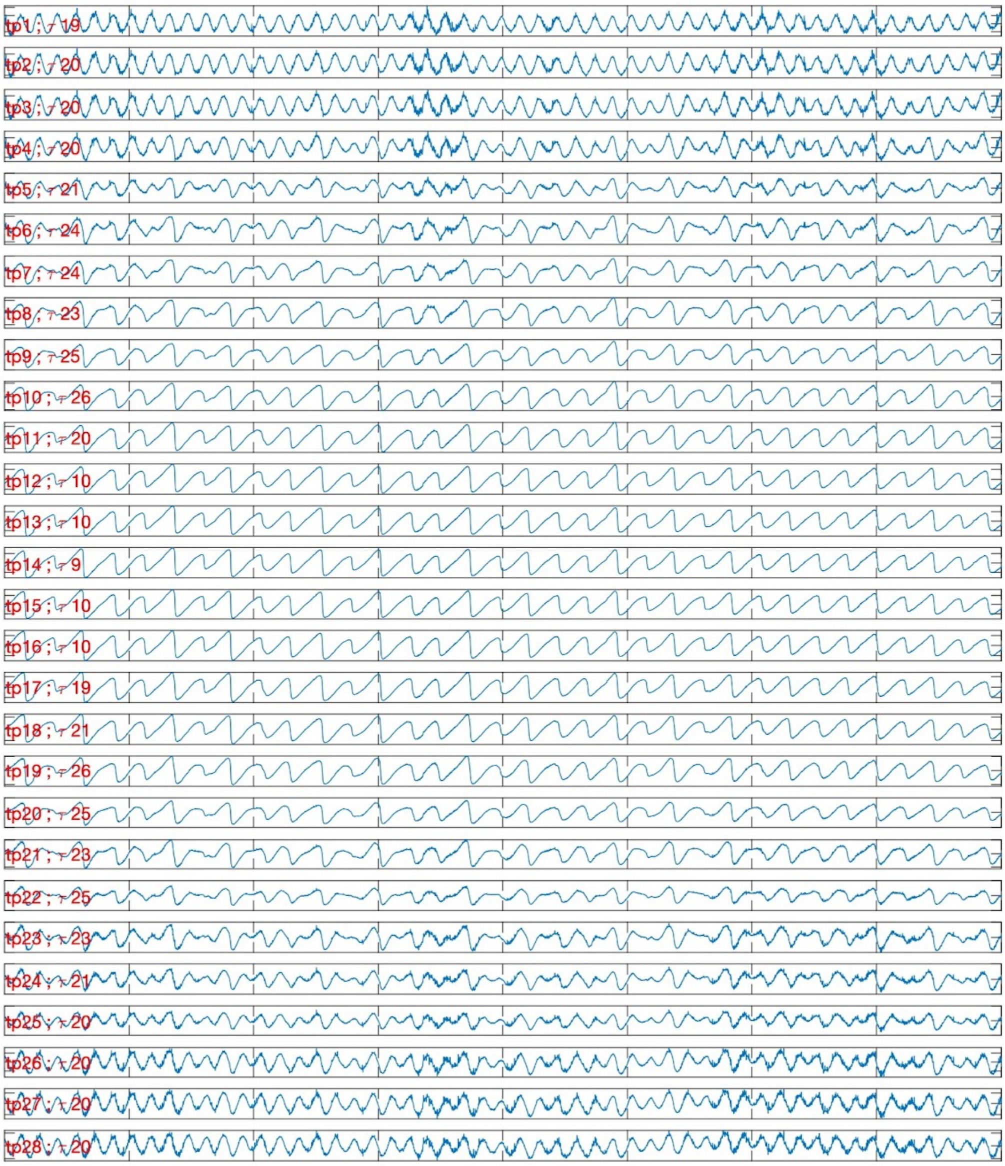

Figure S1: Time series of the trench orthogonal component of displacement for different points along the analyzed cross section from experiment mono gel. Target point number and τAMI are reported within each panel.

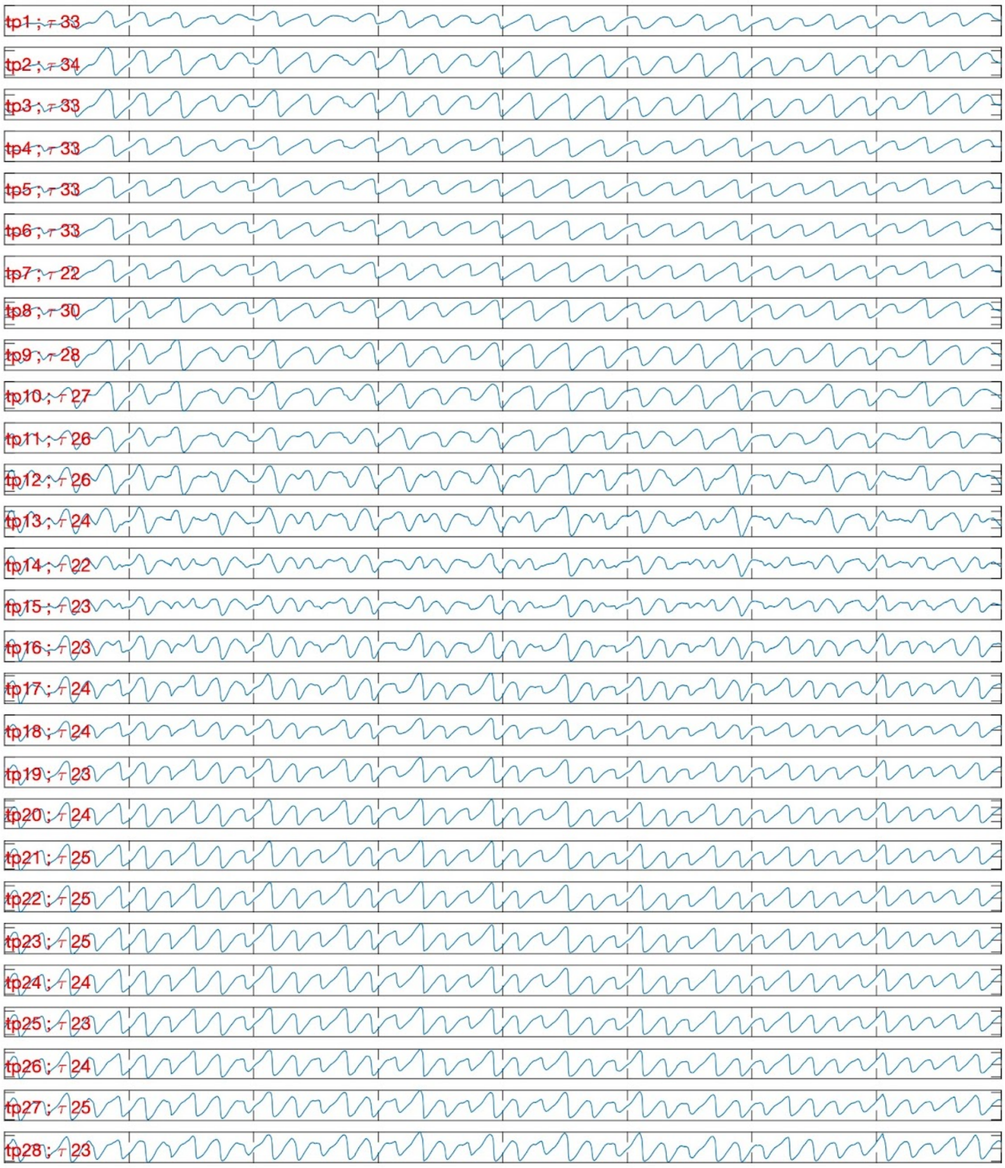

Figure S2: same as figure S1, here for experiment twin gel.

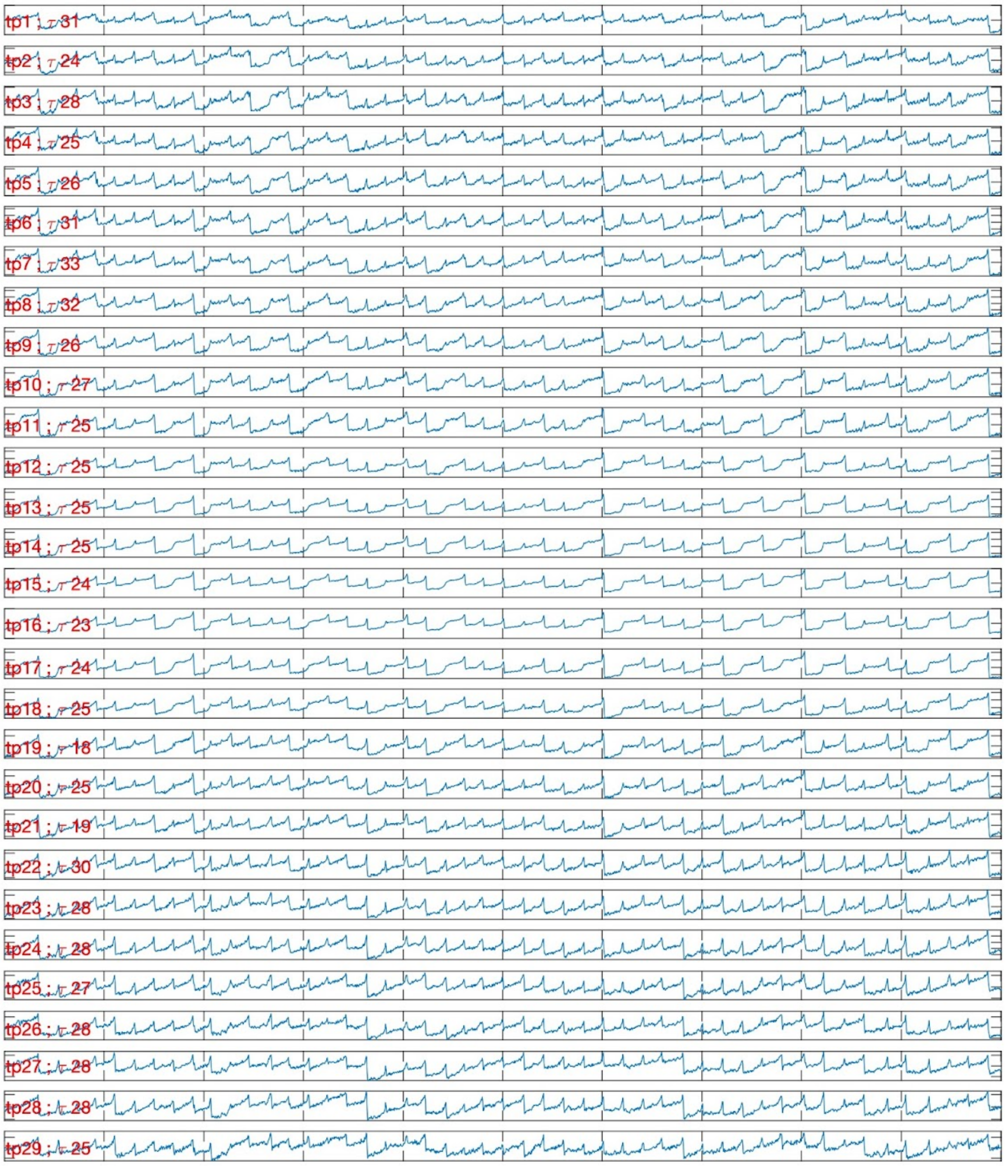

Figure S3: same as figure S1, here for experiment mono foam.

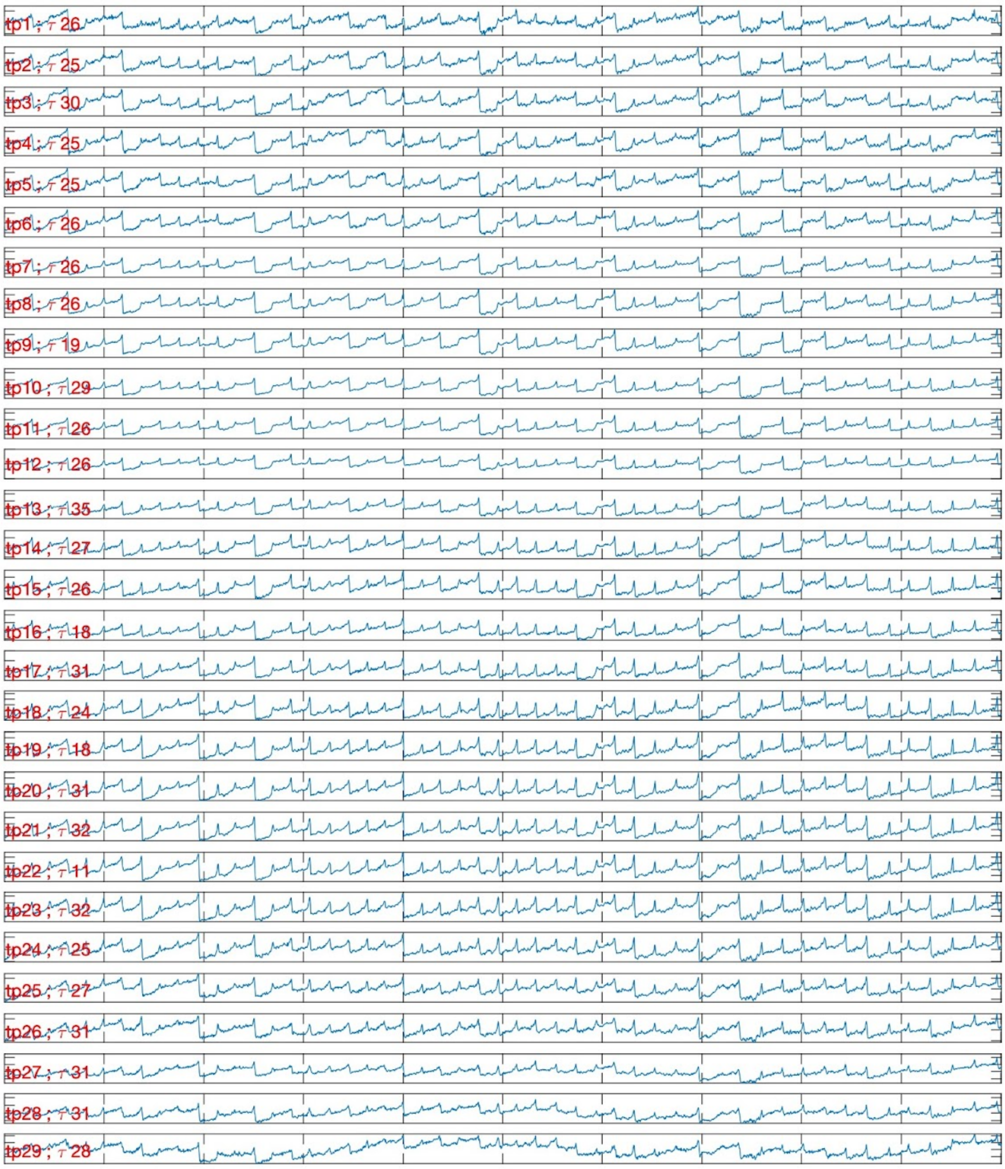

Figure S4: same as figure S1, here for experiment twin foam.

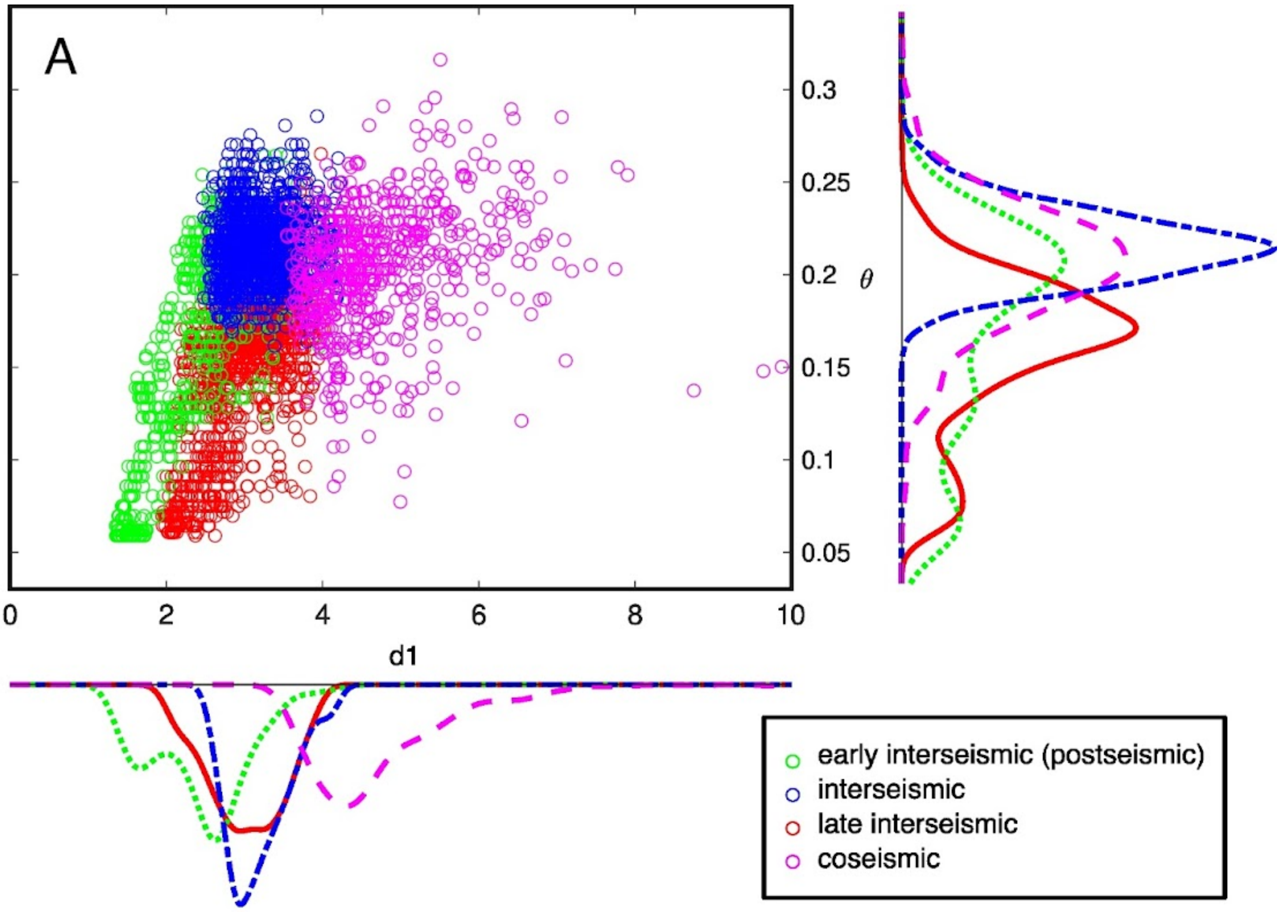

Figure S5: the analog seismic cycle path in the d1, θ space. Marker colors represent different stages of the seismic cycle as identified by k-means analysis to split data into 4 clusters given their distribution in the d1, θ, x space.

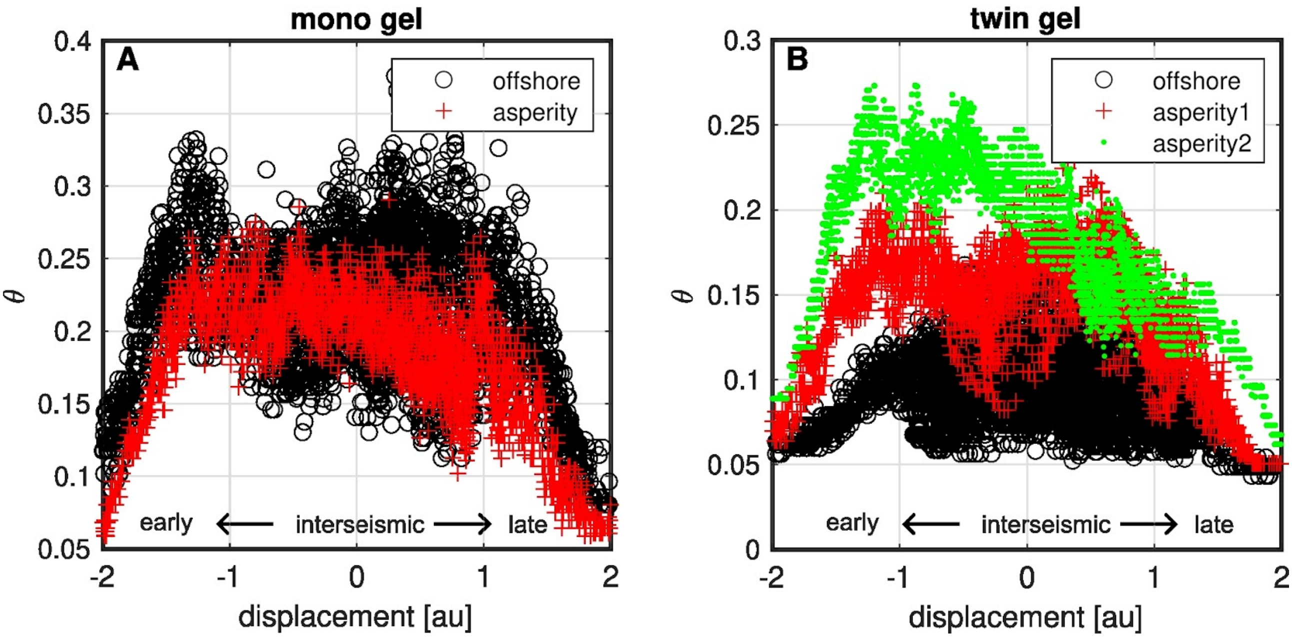

Figure S6: bivariate plot showing the influence of the analyzed area (represented by different markers) on the θ - displacement pattern in Gelquake. We removed all coseismic frames from the analysis so that the axis displacement is representative of different moments into the interseismic period with negative and positive values of displacement corresponding to early and late interseismic, respectively. In twin gel experiment (panel b), a clear decrease of θ in the late-interseismic stage becomes visible only when focusing within individual asperity. Similarly, also in mono gel experiment (panel a) a clearer picture of θ - displacement pattern appears when analyzing the asperity.

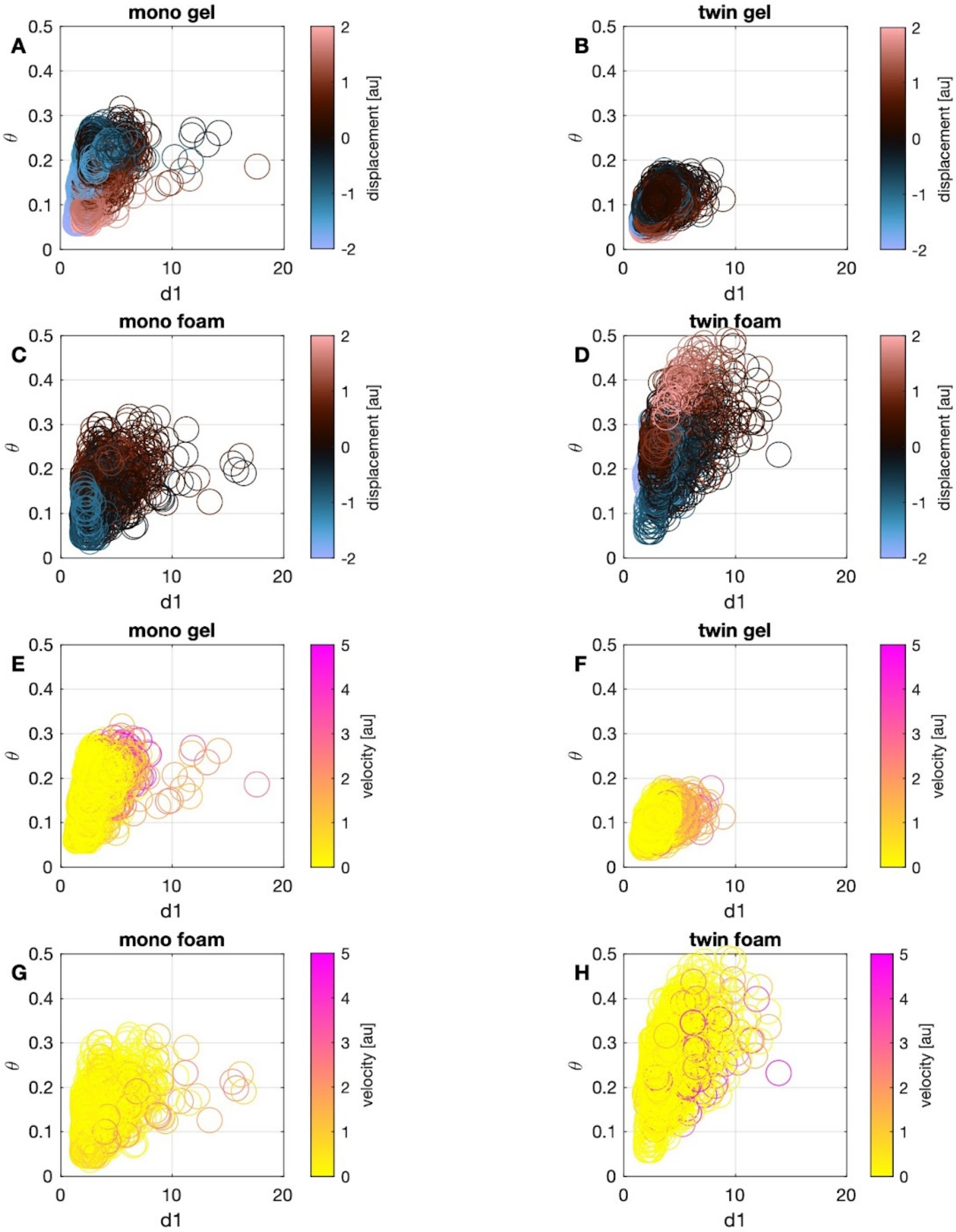

Figure S7: Bivariate plot of d1 against θ colorcoded by displacement (panels a-d) and velocity (panels e-h). Experiment reported as title of each panel.

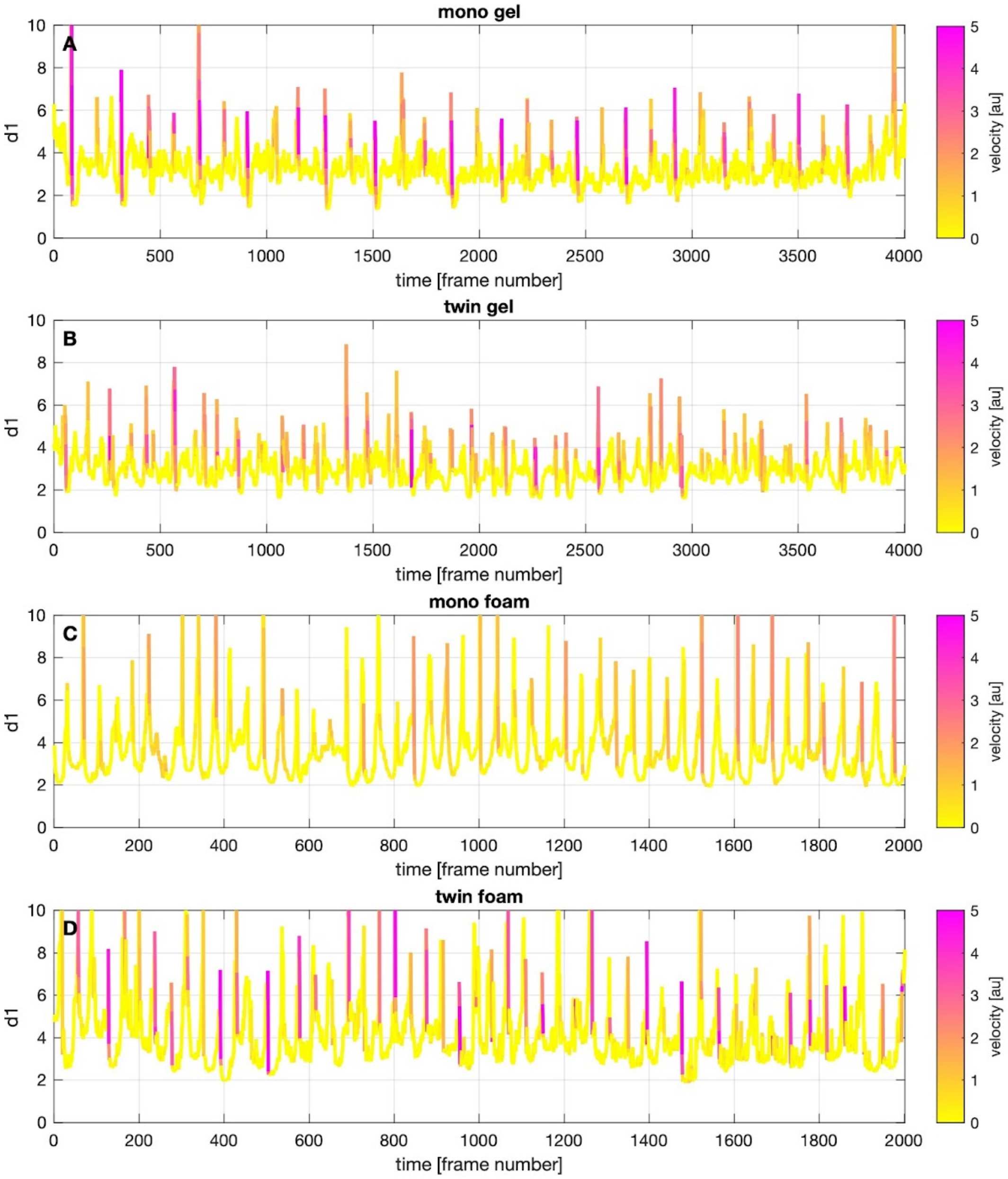

Figure S8: time series of *d1* as a function of time for the analyzed experiments (reported as title in each panel). Time series are colorcoded by velocity. Slip episodes (pinkish colors) correspond to peaks of d1.

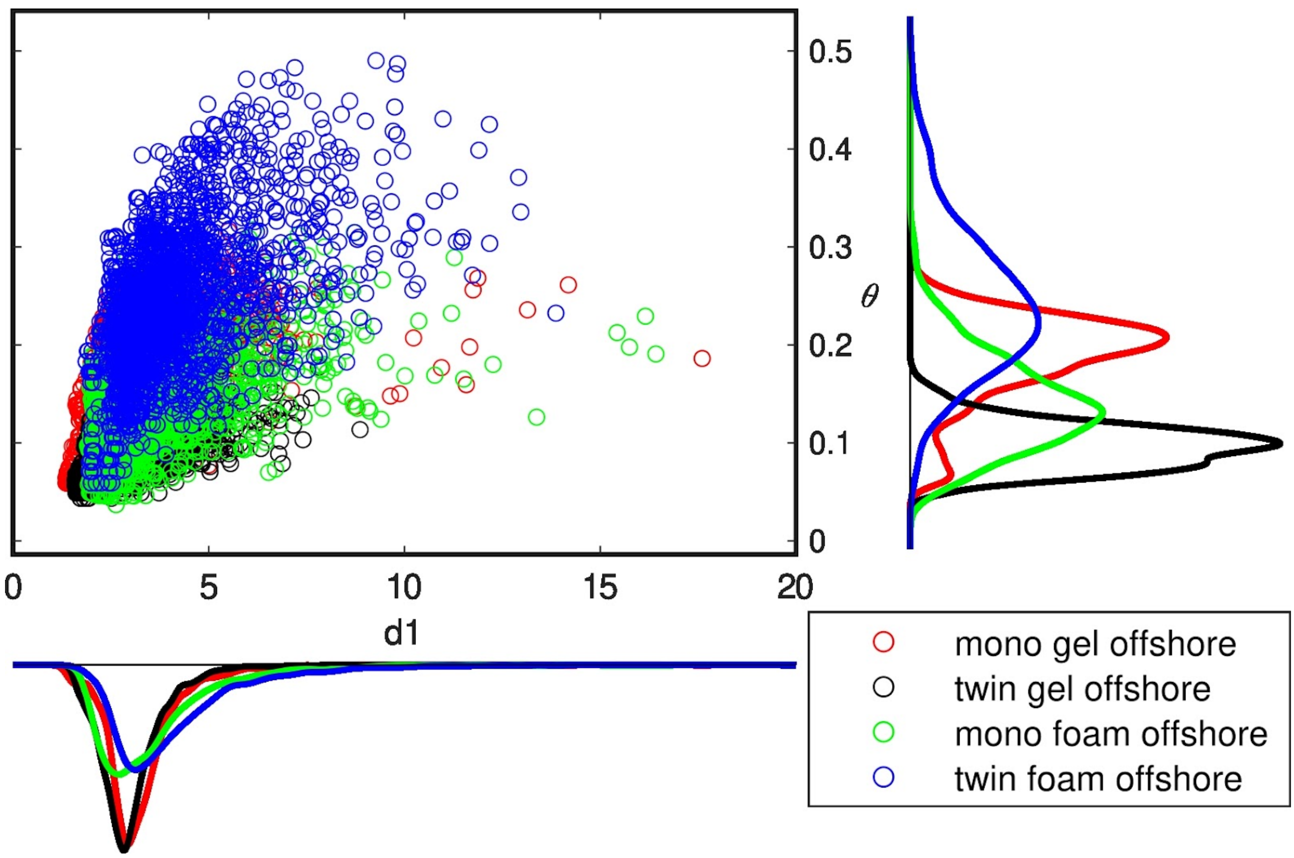

Figure S9: EVT results. Distribution of *d1* and θ for the four experiments used in this study. We notice *d1* distribution similarities by model type rather than by frictional configuration. We also notice that all experiments have remarkably similar minimum values of θ (providing insights of the furthest prediction horizons).

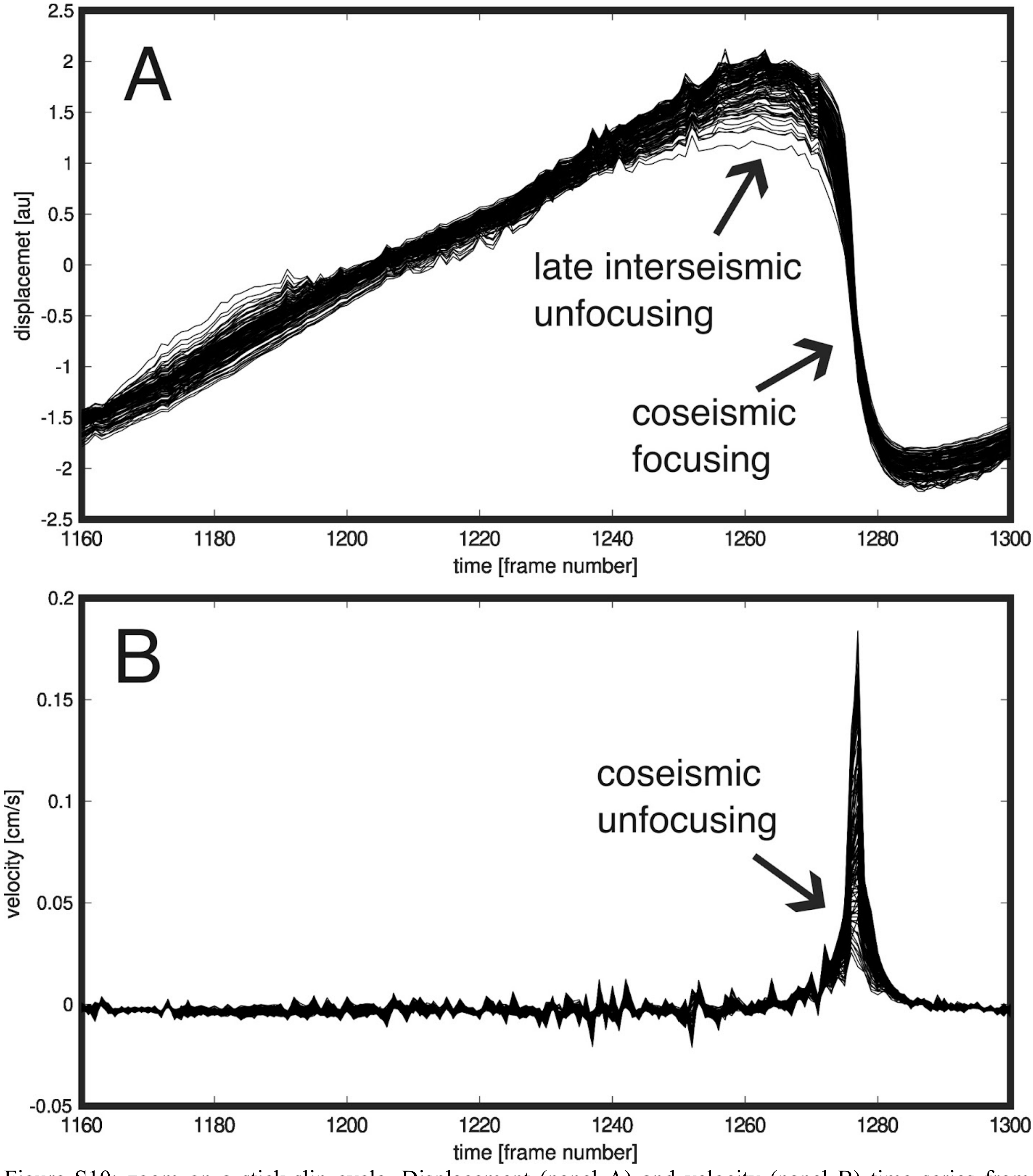

Figure S10: zoom on a stick-slip cycle. Displacement (panel A) and velocity (panel B) time series from measurement points located above the asperity area of model mono gel display different focusing/unfocusing (i.e., concentration of observables at given moment) depending on different stages of the analog seismic cycle.

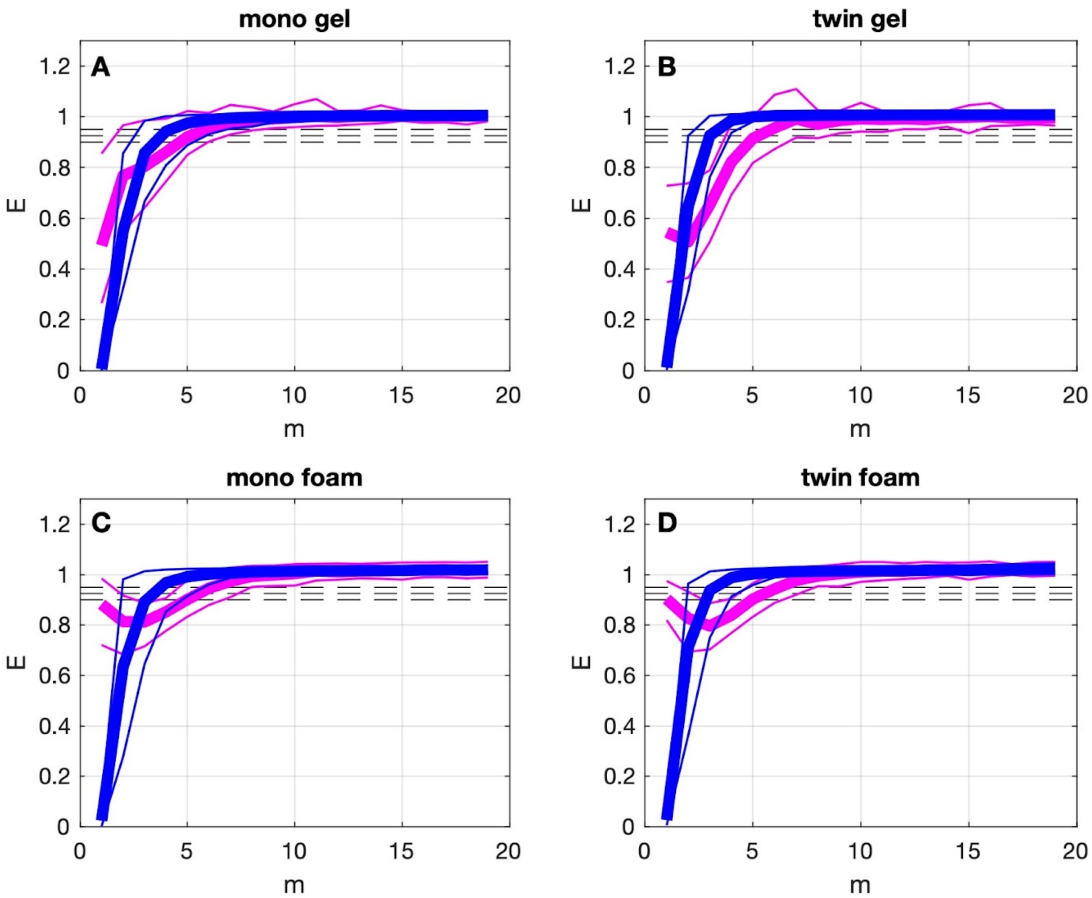

Figure S11: Cao’s method for determining the embedding dimension m. The input signal is the trench orthogonal component of displacement. E_1 (blue lines) and E_2 (magenta lines) as a function of m. Plots summarize the computed values of E_1 and E_2 for different experiments (panel a-d) and all target points along the analyzed cross section. Thick lines represent the mean while thin lines constrain 90% of the data. Black dashed lines represent the three thresholds used in our study.

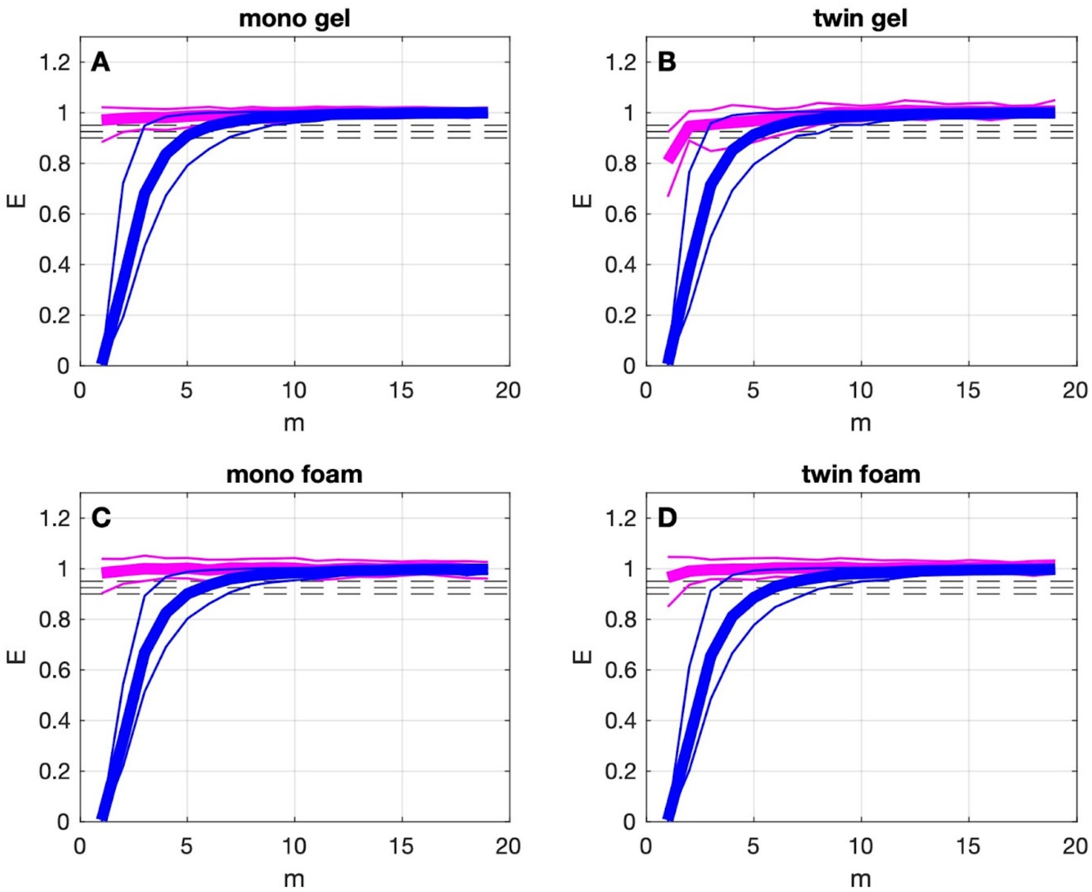

Figure S12: same as figure S11 but using the trench orthogonal component of velocity as signal. Notice, for all experiments, E_2 (magenta) ~ 1 at all tested *m* indicative of a stochastic process.

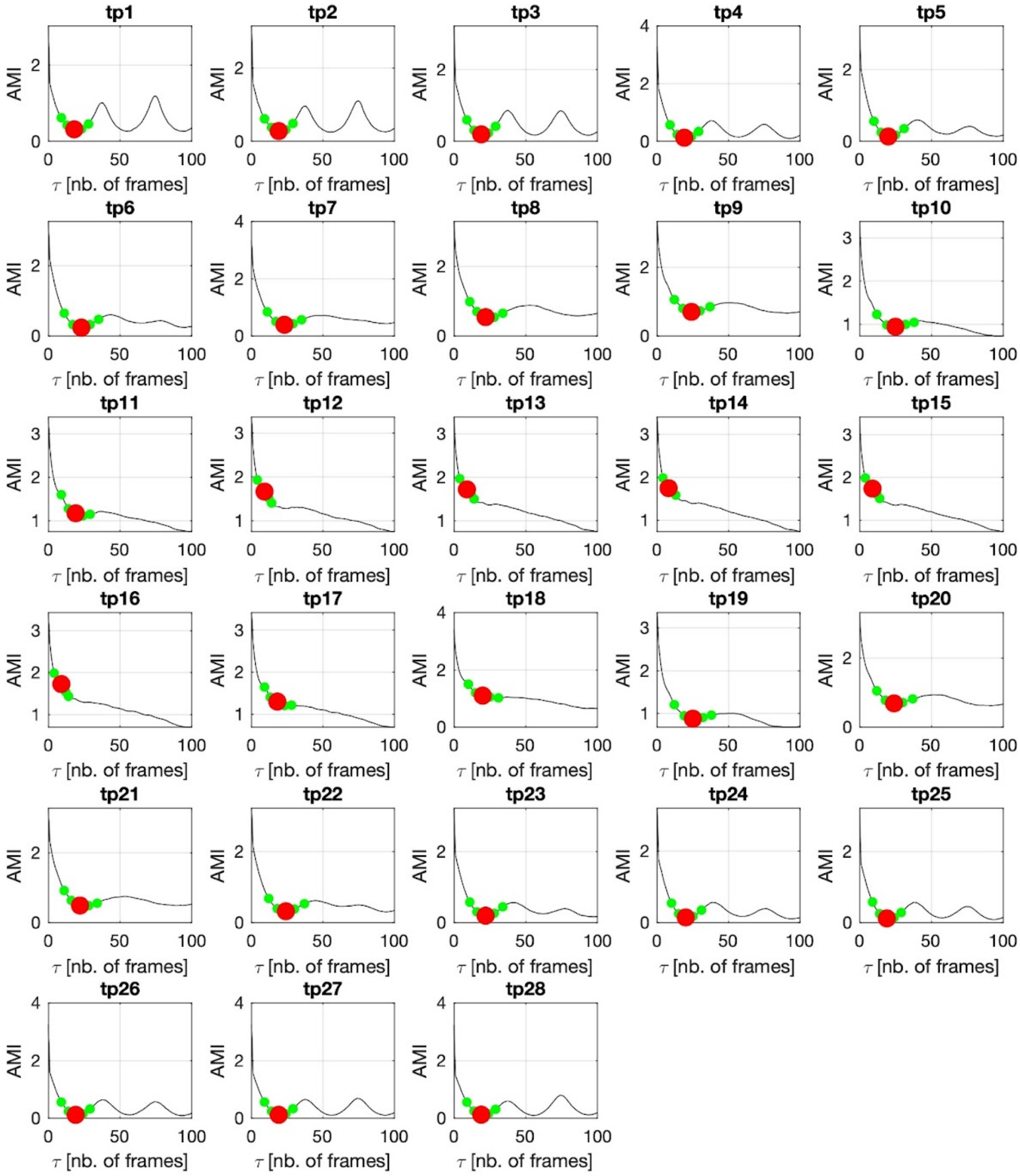

Figure S13: Black curves represent AMI(τ) for different target points tp (reported in titles) for experiment mono gel. Red circles represent the first local minima, i.e., the optimal delay time τAMI. Green circles represent 5 additional, linearly-spaced values of τ in the τAMI/2 - 1.5*τAMI range, that are used to compensate for the potential temporal variation of τ within the investigated time series.

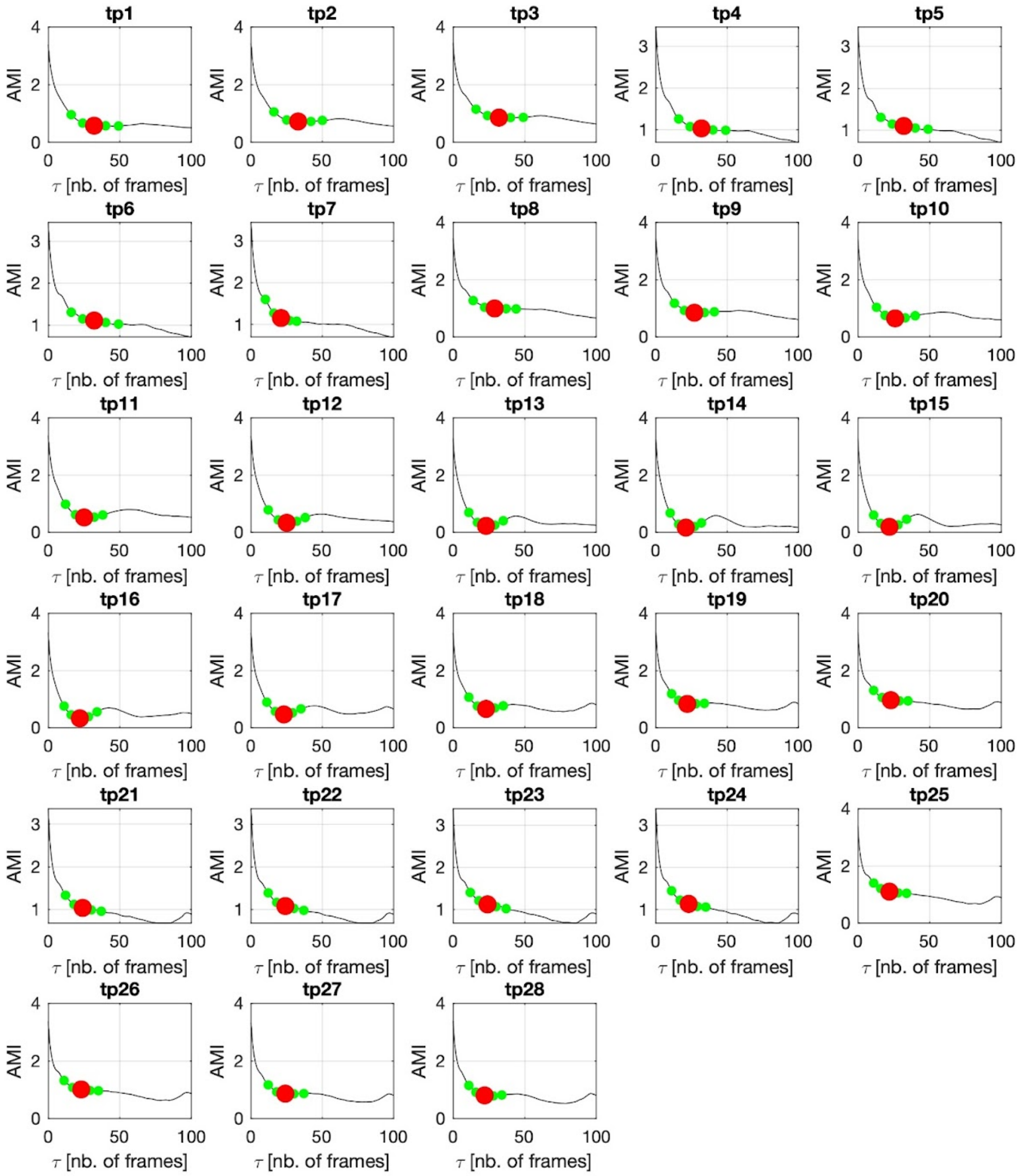

Figure S14: Same as figure S13, here for experiment twin gel.

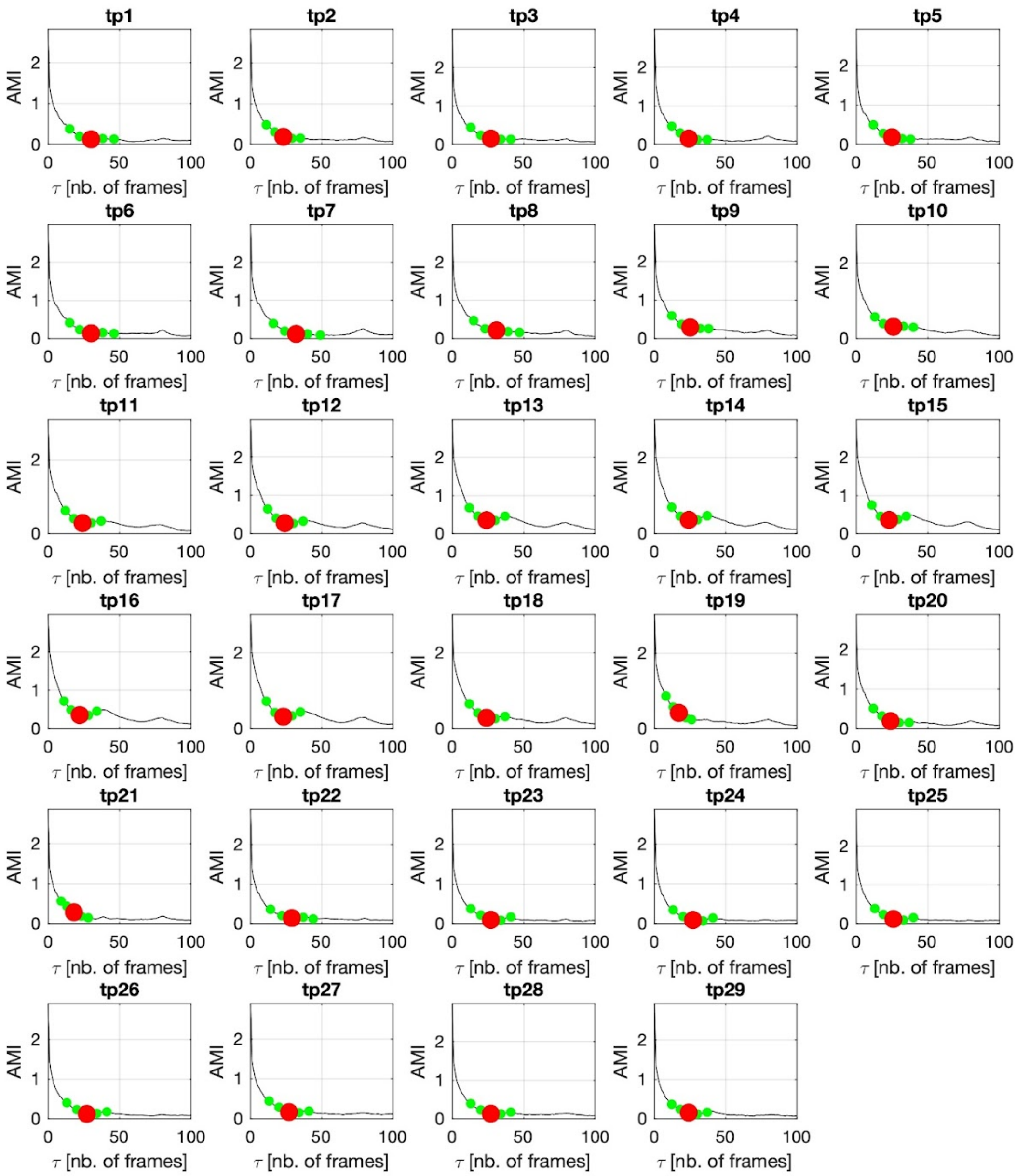

Figure S15: Same as figure S13, here for experiment mono foam.

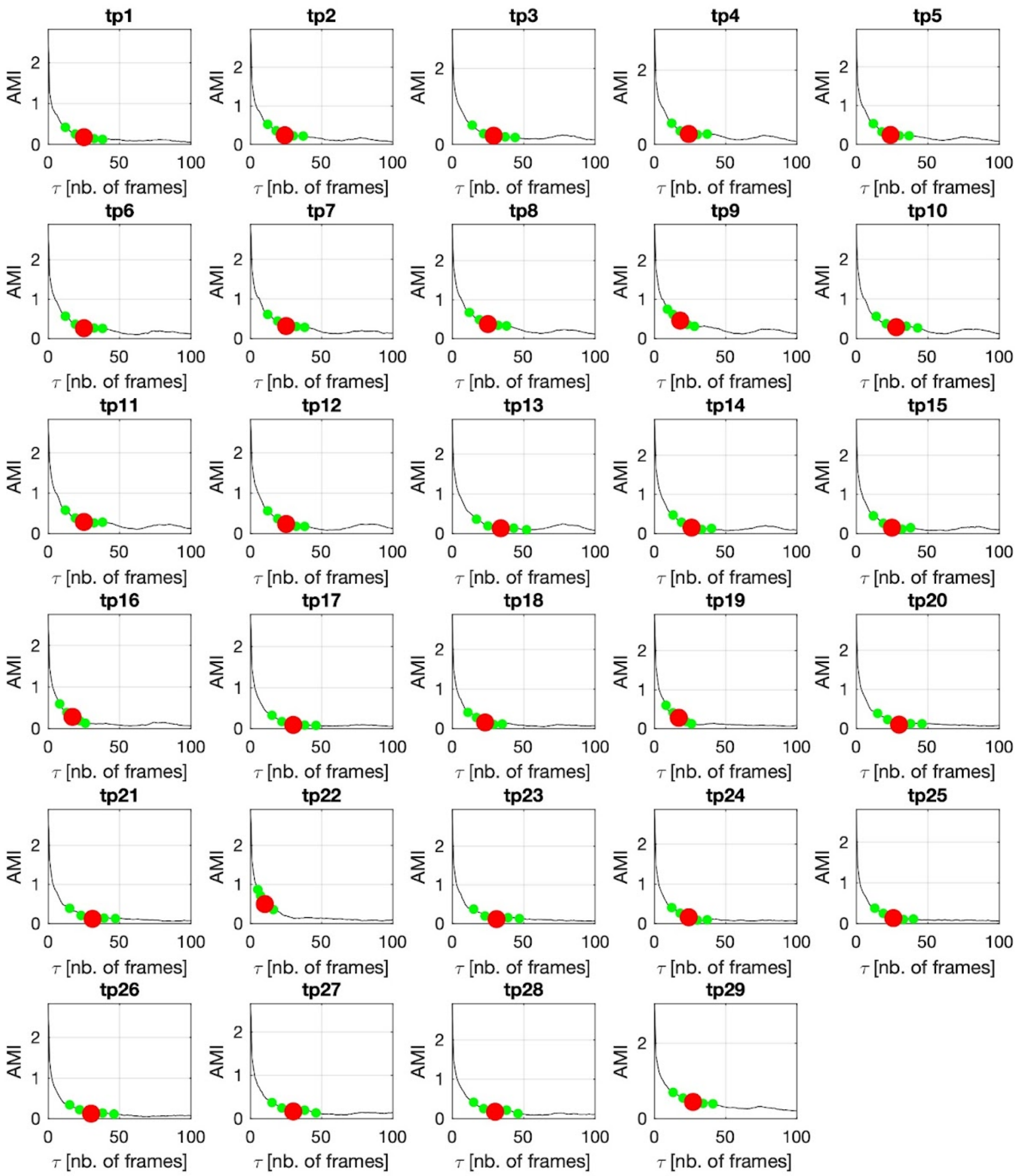

Figure S16: Same as figure S13, here for experiment twin foam.

Table S1: additional information about models and monitoring.

	gelquake	foamquake
images discretization [px^2]	1600 x 1200	2048 x 1536
PIV data size [interrogation windows] (trench orthogonal x trench parallel)	42 x 28	18 X 29
monitoring rate [frames per second]	7.5	50
model dimensions [cm] (x-y plane; trench parallel x trench orthogonal)	34 x 52	150 x 90
length scaling factor (Model/Nature)	1.57×10^{-6} (i.e., 1 cm in the model corresponds to 6.4km in nature)	2.9×10^{-6} (i.e., 1 cm in the model corresponds to 3.5 km in nature)
subducting plate velocity [m/s]	1×10^{-4}	1×10^{-4}
dip of the megathrust [°]	10	10
main reference	Corbi et al. [2013]	Mastella et al. [2022]
number of frames analyzed	4000	2000
number of laboratory earthquakes	34(mono) 67(twin)	50(mono) 49(twin)

REFERENCES

Badii, R., Broggi, G., Derighetti, B., Ravani, M., Ciliberto, S., Politi, A., & Rubio, M. A. (1988). Dimension increase in filtered chaotic signals. *Physical Review Letters*, 60(11), 979-982.

Barraclough, D. R., & De Santis, A. (1997). Some possible evidence for a chaotic geomagnetic field from observational data. *Physics of the Earth and Planetary Interiors*. 99, 3–4. https://doi.org/10.1016/S0031-9201(96)03215-3.

Cao, L. (1997). Practical method for determining the minimum embedding dimension of a scalar time series. *Physica D: Nonlinear Phenomena*, 110(1-2), 43–50.

Corbi, F., F. Funiciello, M. Moroni, Y. van Dinther, P. M. Mai, L. A. Dalguer, and C. Faccenna (2013), The seismic cycle at subduction thrusts: 1. Insights from laboratory models, *J. Geophys. Res. Solid Earth*, 118, doi:10.1029/2012JB009481.

Faranda, D., Messori, G., Yiou, P., (2017). Dynamical proxies of north atlantic predictability and extremes. *Sci. Reports* 7.

Faranda, D., & Vaienti, S. (2018). Correlation dimension and phase space contraction via extreme value theory. *Chaos*, 28(4), 041103.

Farmer A.D., Sidorowich, J.J. (1987). Predicting chaotic time series. *Phys. Rev. Lett*. 59, 845–848.

Gualandi, A., Avouac, J., Michel, S., & Faranda, D. (2020). The predictable chaos of slow earthquakes. *Science Advances*, 6. https://doi.org/10.1126.

Lorenz, E.N. (1969). Atmospheric predictability as revealed by naturally occurring analogues. *Journal of the Atmospheric sciences*. Sciences;26(4):636-46.

Mastella, G., Corbi, F., Funiciello, F., & Rosenau, M. (2022). Foamquake: A novel analog model mimicking megathrust seismic cycles. *Journal of Geophysical Research: Solid Earth*, 127(3). https://doi.org/10.1029/2021JB022789

Sauer, T., Yorke, J.A., and Casdagli, M. (1991). Embedology, *Journal of Statistical Physics*, Vol. 65, Nos. 3/4, doi: 0022-4715/91/1100-0579506.50/0.

Suveges M. (2007) Likelihood estimation of the extremal index. *Extremes* 10:41–55 DOI 10.1007/s10687-007-0034-2

Takens F., Detecting Strange Attractors in Turbulence, in Lecture Notes in Mathematics (Springer, ed. 2, 1981), p. 366.

Theiler, J., & Eubank, S. (1993). Long-term prediction: A nonlinear dynamics perspective. In Proceedings of the IEEE International Conference on Neural Networks (Vol. 4, pp. 1458-1463).

Wales, D.L. (1991) Calculating the rate of loss of information from chaotic time series by forecasting. *Nature* 350, 485–488 (1991)